applied sciences

MDPI

Article

A Nonlinear Energy Sink Design to Attenuate the Torsional Oscillations of Lightly Loaded Gear Pairs

Brett Friskney [1], Panagiotis Alevras [2], Sourabh Londhe [1], Stephanos Theodossiades [1,*] and Donald Michael McFarland [3]

[1] Wolfson School of Mechanical, Electrical and Manufacturing Engineering, Loughborough University, Loughborough LE11 3TU, UK; b.t.friskney@lboro.ac.uk (B.F.); londhesourabh@gmail.com (S.L.)
[2] Department of Mechanical Engineering, School of Engineering, University of Birmingham, Birmingham B15 2TT, UK; p.alevras@bham.ac.uk
[3] Sound and Vibration Laboratory, College of Mechanical Engineering, Zhejiang University of Technology, Hangzhou 310014, China; dmmcf@illinois.edu
* Correspondence: S.Theodossiades@lboro.ac.uk

Abstract: Nonlinear energy sinks (NES) have recently attracted significant interest for the suppression of unwanted vibrations in a variety of mechanical systems. The key advantage in employing this (vibration absorber) approach is the broadband nature of the interactions with a primary system for which vibration energy dissipation is required. Thus, the effectiveness of the NES is decoupled from the need of tuning to specific frequencies. Nevertheless, NES for rotational fluctuations of powertrains have received limited attention in the literature. In this work, a design for a rotational NES to mitigate speed fluctuations in gear trains is presented and tested experimentally. The development of the proposed system is underpinned by previous optimisation studies conducted by the authors, where a disk was utilised as an inerter NES. A set of beams couple the inerter with the wheel gear of a spur gear pair with a nonlinear restoring torque, which is designed to approach the desired essential nonlinearity within realistic practical tolerances. Static and dynamic identification is conducted to confirm the desired characteristics. Despite uncertainties in the prototype testing, the approach is found to reduce the speed fluctuations on the gear pair output shaft, with appropriate predictability established for the model and the design procedure.

Keywords: nonlinear energy sink; torsional oscillation; gear pairs; targeted energy transfer; nonlinear stiffness; thin beam springs

Citation: Friskney, B.; Alevras, P.; Londhe, S.; Theodossiades, S.; McFarland, D.M. A Nonlinear Energy Sink Design to Attenuate the Torsional Oscillations of Lightly Loaded Gear Pairs. *Appl. Sci.* **2022**, *12*, 6778. https://doi.org/10.3390/app12136778

Academic Editor: Giuseppe Lacidogna

Received: 25 May 2022
Accepted: 29 June 2022
Published: 4 July 2022

1. Introduction

The strict regulations for reduced emissions have driven the automotive industry towards developing downsized, turbo-charged engines with higher fuel efficiency. The drawback is the generation of aggressive drivetrain torsional oscillations due to the increased power to weight ratio [1]. A common by-product of drivetrain oscillations that penetrate the transmission is gear rattling noise [2,3], which is predominantly radiated due to the impacts of the unloaded (non-engaged) gear pairs. To overcome the adverse effects of gear rattling noise on vehicle quality perception, expensive and sizeable palliatives tuned to certain frequency ranges (such as dual-mass flywheels, clutch pre-dampers and centrifugal pendulum absorbers) [4,5] are employed by automotive manufacturers. Nevertheless, because of the tuning conditions, these palliatives do not act in a broadband manner over the powertrain response.

Recent studies [6–11] have revealed the potential of using nonlinear vibration absorbers (nonlinear energy sinks (NES)) with low mass and inertia properties for effectively attenuating the generation and propagation of powertrain torsional oscillations. The NES possesses essentially nonlinear stiffness and, thus, instead of being tuned to a preferential frequency, it is activated by the energy input. This is the concept of targeted energy transfer

(TET) (also known as energy pumping), whereby the oscillatory energy is transferred in a nearly irreversible manner from a primary system donor (drivetrain) to a secondary system receiver (NES) [12], where it is then either redistributed within the modal domain or locally dissipated. Numerous publications in the literature have been dedicated to understanding, designing and optimising NES vibration absorbers by studying the underlying dynamics [13–18]. The vast majority of works concern absorbers that are acting in translational motion and comprise investigations where an NES was implemented on reduced-order primary system models [13,14]. The dynamics of energy pumping in systems equipped with an NES have been systematically investigated by parametric studies of the system's main properties [15], whereas studies have considered both grounded and ungrounded NES absorbers [16,17] to understand their nonlinear dynamics and the NES effectiveness. The activation of nonlinear normal modes (NNMs) has been also discussed [18] to illustrate how the NES may interact with the primary system.

More recently, NES mechanisms have been studied for passive structural control purposes and were shown to effectively dissipate energy from structural systems during oscillatory operating conditions. Time-domain numerical methods have been utilised due to the geometric nonlinearities of the NES [9,19]. An NES with an inerter (NESI) for passive vibration control has been presented [20,21], converting relative translational motion to rotational motion. The small physical mass of the inerter is an advantage, potentially enabling the NESI to provide comparable vibration attenuation to an NES that possesses a larger physical mass. An alternative NES configuration has been proposed utilising bi-stability (BNES) with buckled beams to suppress the oscillations of unbalanced rotor systems [22]. The numerical simulations have been verified by experimental work to confirm the performance of the BNES. The results showed that the BNES can effectively deal with varied energy quantities.

Nevertheless, a limited number of studies involving rotational NES have been reported in the literature. A torsional NES was proposed in [23] to stabilise a rotational drilling system. The dynamics of a rotational NES mounted within a linear oscillator were studied in [24]. The suppression of torsional aeroelastic instabilities on a flexible wing was examined experimentally using a rotational NES that was housed on the tip of the wing [25]. Steel wire was employed as a mechanism for generating cubic force nonlinearity. The effectiveness of using individual and paired NES in suppressing broadband torsional vibrations in automotive powertrains connected to a turbo-charged engine was examined theoretically in [6,7]. The capability of NES to attenuate automotive powertrain torsional oscillations by energy redistribution and dissipation was demonstrated in a numerical study [8]. The design of NES for attenuating the torsional oscillations of propulsion systems was shown experimentally [9]. A theoretical analysis involving a spur gear pair coupled with a rotary NES has been presented [26], showing that targeted energy transfer (TET) can be activated, introducing quasiperiodic motion. The effect of NES mounted on a spur gear pair that operates at low, harmonically varying operating loads (resembling rattling conditions of transmission unloaded gears) has been studied theoretically to demonstrate the performance of the NES in attenuating the gear's torsional oscillations [27]. In this paper, a rotational NES prototype utilising thin shims is experimentally tested. The device is shown to effectively reduce the output speed fluctuations of a lightly loaded spur gear pair.

2. Materials and Methods

The numerical model that is used in this paper has been presented in detail in Friskney et al. [27]. For completeness, we reiterate some of the key aspects and findings from this previous work. Figure 1 shows a sketch of the meshed gears with an NES attached on the gear.

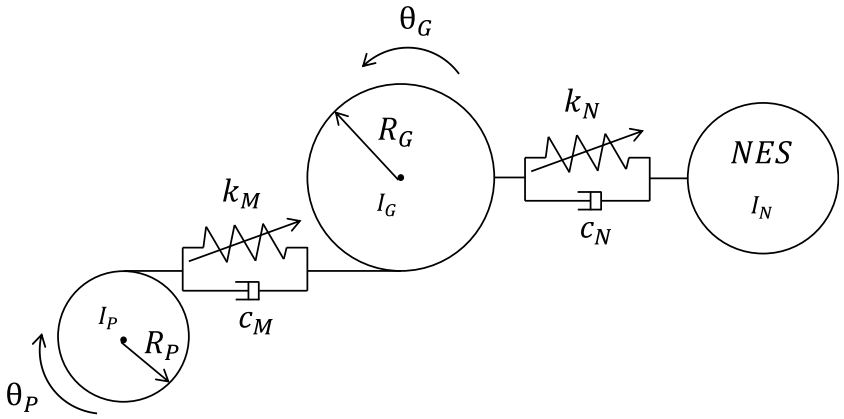

Figure 1. Sketch of the general layout of a gear pair equipped with an NES; I_P represents the pinion, I_G represents the gear; I_N represents the NES; k_M denotes the gear pair meshing stiffness and k_N the stiffness of the NES attachment.

The equations of motion of the system shown in Figure 1 are given in Equations (1)–(3) below. The reader is referred to previous work [27] for a comprehensive description and detailed documentation of the model parameters. Note that the model parameters are informed by the experimental setup that is used in the current work, and therefore the interested reader is referred to [27] for the gear pair setup details.

$$I_p\ddot{\theta}_p + R_pC_M\dot{x}_t + R_pK_Mx_t = T_p + T_f\cos\omega t, \tag{1}$$

$$I_G\ddot{\theta}_G - R_pC_M\dot{x}_t - R_GK_Mx_t + K_N(\theta_G - \theta_N)^3 + C_N\left(\dot{\theta}_G - \dot{\theta}_N\right) = -T_G, \tag{2}$$

$$I_N\ddot{\theta}_N - K_N(\theta_G - \theta_N)^3 - C_N\left(\dot{\theta}_G - \dot{\theta}_N\right) = 0 \tag{3}$$

where $\ddot{\theta}_{G,P,N}$, $\dot{\theta}_{G,P,N}$, $\theta_{G,P,N}$ denote the angular acceleration, velocity and position of the gear (subscript G), the pinion (subscript P) and the NES (subscript N), respectively. R_P is the pinion radius, R_G is the gear radius, T_P is the pinion average torque, T_f is the pinion fluctuating torque of angular frequency ω and T_G is the gear torque. The time-varying meshing stiffness is a function of the angular position of the pinion and the applied torque and it is denoted by K_M. The mesh displacement x_t is described by a piecewise linear function with backlash [27]. The damping coefficient in the pinion–gear contact is C_M, and the NES damping coefficient is denoted by C_N, whereas the NES nonlinear stiffness coefficient is $K_N = k_3$, where an essentially cubic nonlinearity is assumed.

Rich information for establishing targeted energy transfer in a primary system with an NES is contained in the NNMs of the coupled nonlinear system of oscillators. However, the piecewise linear profile of the gear teeth deflection induced by the presence of backlash introduces difficulties in attaining the NNMs. In order to mitigate computational difficulties, the backlash is ignored in the calculation of the NNMs, leading to a constant average meshing stiffness, without, as will be found in the experimental results, affecting the conclusions drawn. Figure 2 shows the NNMs of the gear pair with an NES possessing a cubic stiffness of $k_3 = 430\ \mathrm{Nm/m^3}$, as informed by optimising the NES properties using the presented model [27].

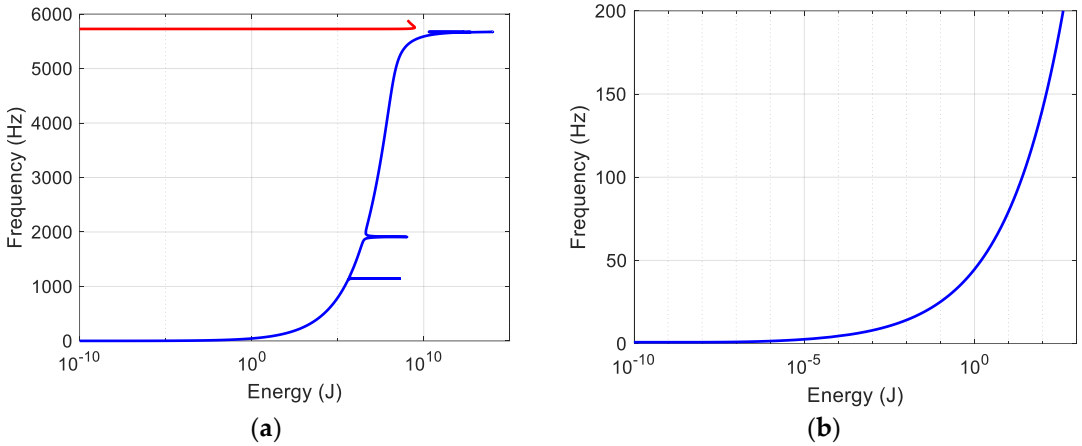

Figure 2. (**a**) NNMs without the rigid body mode and using the average meshing stiffness; (**b**) zoom-in for the first mode in the experimentally observed frequency range.

The NNM corresponding to the primary system (gear pair) is the one resulting from the meshing stiffness. Due to the very high value of this stiffness, the resulting NNM exists at very high frequencies (solid red line in Figure 2a), far away from the frequency ranges typically observed in the speed fluctuations of automotive driveshafts. On the other hand, the essential nonlinearity of the NES stiffness sweeps through the entire frequency range depending on the vibration energy. Closer observation of this NNM in the frequency range of interest (up to 200 Hz) in Figure 2b reveals the NES frequency coverage that motivates this experimental study to reduce gear speed fluctuations by the action of an NES attachment. Previous modelling work [27] has shown that the inclusion of the NES in the gear pair results in a promising reduction in the gear fluctuations that is linked to the gear rattling root cause. Figure 3 shows the modelled reduction in the gear speed amplitude when the NES is included ("active" result) with respect to the corresponding amplitude without the NES ("locked" result) across the speed range that is achievable in the experimental gear pair setup. Note that the NES is attached to the gear in both scenarios, but it is restrained from oscillating in the locked case in order to eliminate an inertia bias in the comparison of the results.

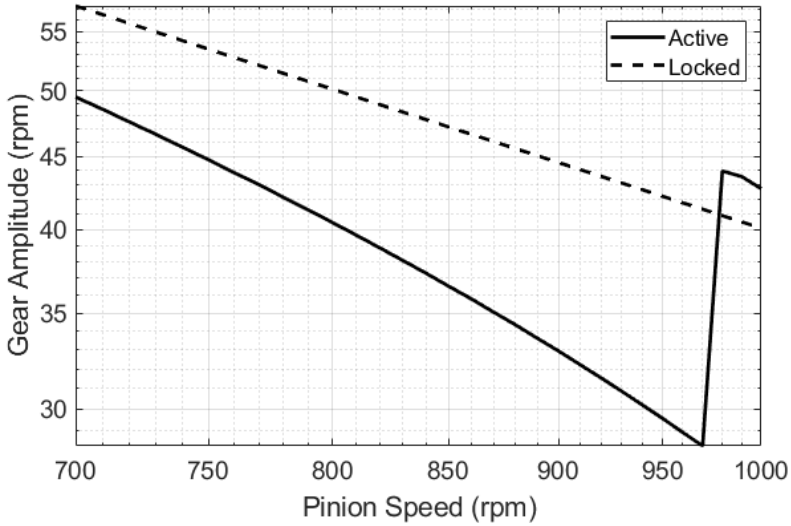

Figure 3. Numerical frequency response curve for k_N = 430 Nm/rad^3.

The NES assembly has been designed in order to physically realise the predicted force–deflection profile. Different views of the NES assembly are shown in Figure 4. The mechanism to achieve the desired stiffness nonlinearity is by the deflection of steel

shims as the rocker oscillates about its mean position, producing a reactionary torque. The latter is rigidly mounted on the rotating shaft that is connected to the primary (host) system. As the rocker deflects the shims, the NES inertia disc (made of aluminium) is engaged, accepting energy from the primary system. The NES disc hosts the shim mounts and itself is mounted on the rotating shaft (of the primary system) through a bearing connection so that it can freely rotate with respect to the shaft. Deep groove ball bearings have been used to reduce friction between the shaft and the NES disc. Each shim is fixed at its end mounts and assembled so that it is in contact with a brass roller. The rocker rotation moves the rollers, deflecting the shims.

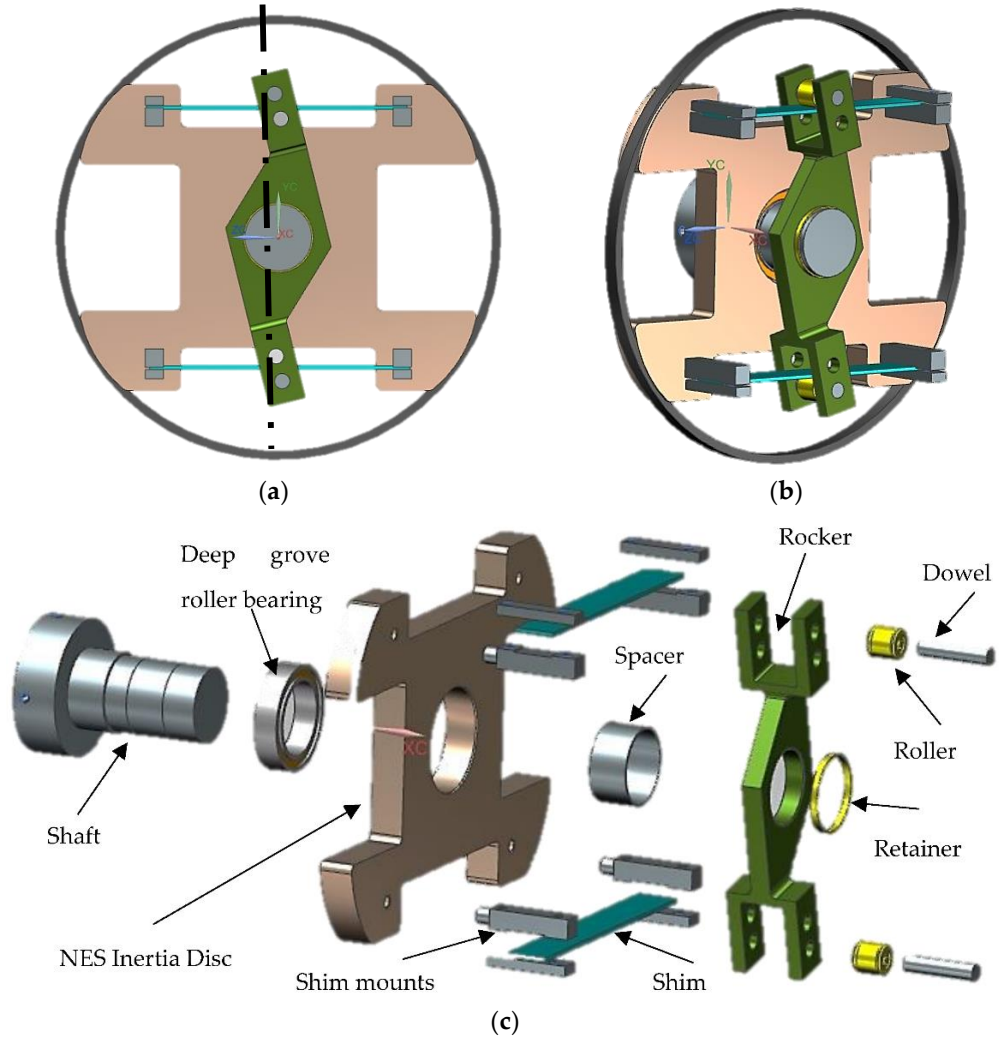

Figure 4. (**a**) Front, (**b**) inclined and (**c**) exploded CAD views of the NES assembly.

The force that is deflecting the shims is calculated using beam bending theory, considering that the shims are fixed at both ends and eccentrically loaded. The key assumptions are as follows:

- The beam is straight (i.e., it has no curvature);
- The beam material elasticity is the same in both tension and compression;
- The stress in the beam is below the elastic limit;
- The deflections are small;
- The beam undergoes pure bending;
- The friction between the rocker and shim is small (the NES damping will be identified experimentally in a later section);
- It is assumed that the rocker touches the shim at a single point of contact.

The configuration of the shim is shown in Figure 5 for unloaded and loaded scenarios. The total length of the rocker arm is 2 h (see Figure 5a), the length of the shim between the mounts is L and, initially, the roller is situated at the shim's midpoint (unloaded scenario). The shims have a rectangular cross-section with width (w) and thickness (t). Following some counter-clockwise rotation of the rocker by angle θ, the new rocker position is as shown in Figure 5b as A'B'. Using beam bending theory, the force applied at each shim is given by:

$$F = \left[\frac{3\,L^3 E\,I}{a'^3\,b'^3}\right] \times dy \tag{4}$$

where $a' = \frac{L}{2} + dx$, $b' = \frac{L}{2} - dx$, $dy = h(1 - \cos(\theta))$, $dx = h\,\sin(\theta)$ and E is the is modulus of elasticity for steel, while I is the second moment of area $\left(w\,t^3/12\right)$. Values for the abovementioned parameters are provided in Table 1.

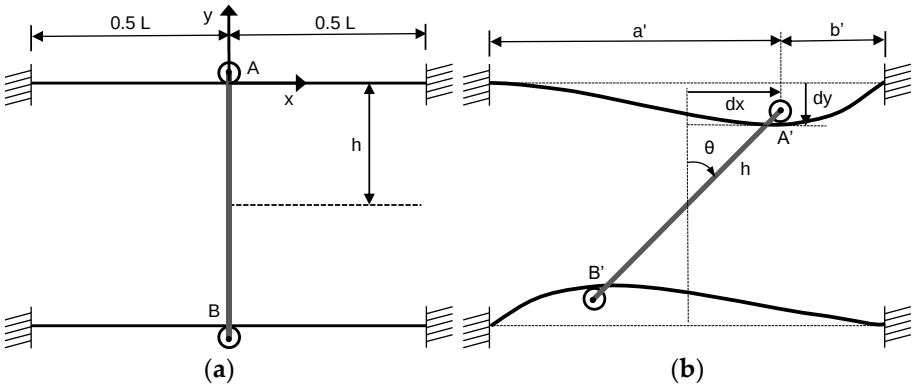

Figure 5. (**a**) Unloaded and (**b**) loaded snapshots of the NES shims.

Table 1. Material and geometrical properties of the NES shims.

Parameter	Value
Modulus of elasticity (*E*)	2×10^{11} N/m^2
Shim thickness (t)	0.0012 m
Shim width (w)	0.012 m
Shim length (L)	0.076 m
Half-length of the rocker arm (h)	0.047 m

The centrifugal force generated on the shim during the assembly rotation is negligible; hence, it will be ignored. The direction of the force is parallel to the y-axis at point A′. As a result, the torque applied on the rocker due to deflection angle θ on both shims is given by:

$$T = 2F \times dx \tag{5}$$

The above expression describes the torque as a function of the deflection angle θ and will be validated both statically and dynamically. The expansion of the torque expression in a Taylor series with the trigonometric terms considered up to the fifth order gives the following expression for the quintic (essentially) nonlinear stiffness function:

$$T_{NL} = k_3 \times \theta^3 + k_5 \times \theta^5 \tag{6}$$

with $k_3 = \frac{192\,h^2 E\,I}{L^3}$, $k_5 = \frac{48EIh^2\left(\,48h^2 - L^2\,\right)}{L^5}$.

Previous modelling work that was briefly described in Section 2 has considered purely cubic stiffness; however, practical realisations that would eliminate the quintic term were found hard to implement. Therefore, the quintic term was retained in the nonlinear NES torque design, aiming for the torque given by Equation (6) to approach the theoretical

cubic torque as much as feasible. Using the values in Table 1, the stiffness coefficients are calculated as $k_3 = 334$ Nm/rad^3 and $k_5 = 1449$ Nm/rad^5. Figure 6 shows a comparison of the theoretical target torque with the designed torque given by Equation (5) and with its Taylor expansion given by Equation (6). The quintic expansion shows excellent agreement with the designed torque for the examined angle range, which makes it reasonable to drop terms of higher order. Furthermore, a small deviation from the originally targeted torque profile is observed, which, nevertheless, is too small to cause any concern regarding the effect of the NES on the gear amplitude.

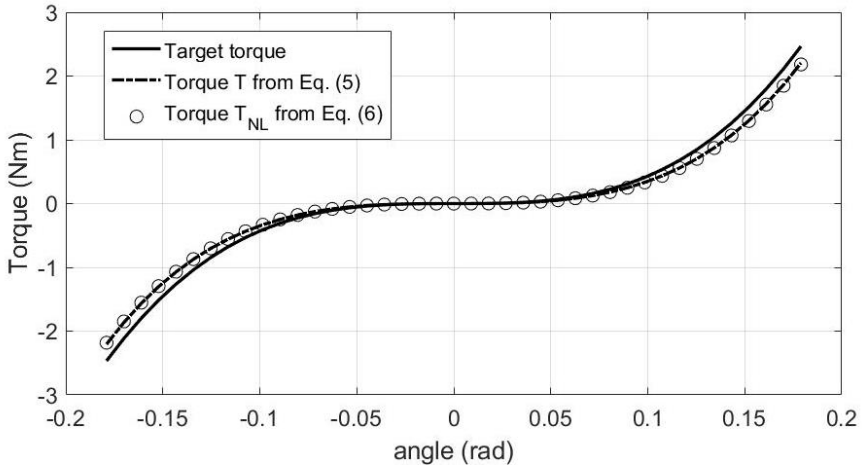

Figure 6. Target torque ($k_3 = 430$ Nm/rad^3) versus theoretical torque model of the NES given by Equation (5) and corresponding Taylor expansions up to 5th order given by Equation (6).

In order to establish robust TET conditions between the NES and the primary (host) system, the NES damping content has to be as low as possible so that it does not contaminate the essentially nonlinear force. Thus, the friction between the dowel and roller surfaces should be low to favour pure rolling motion. To achieve this, the NES roller assembly should be lubricated. A roller bearing with a low friction coefficient is an attractive alternative and it has been employed in this work. This bearing type can exhibit a static coefficient of friction between 0.002 and 0.005, whereas the kinetic friction coefficient can vary between 0.001 and 0.0018.

3. Results

This section presents an experimental study of the gear amplitude reduction achieved by attaching an NES to a gear pair assembly.

3.1. Experimental Setup

The experimental study was conducted using the apparatus shown in Figure 7a. An electric motor was installed on an isolated optical table and manually controlled through an inverter. The motor shaft was attached to the shaft of a pinion gear using two elastic couplings, between which a torque sensor was inserted. A single-stage spur gear pair with a ratio of 2:1 was driven by the electric motor. Details of the gear pair are provided in Table 2 along with the values of the applied torque profile.

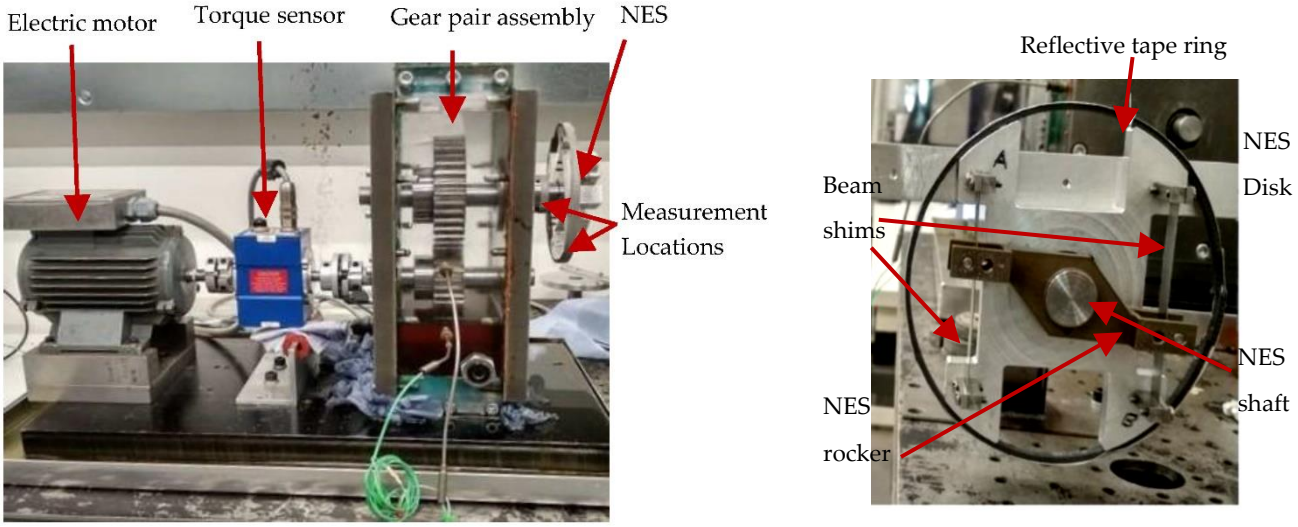

Figure 7. (**a**) Experimental setup; (**b**) NES disk.

Table 2. Parameters of the gear assembly.

Parameter	Value
Inertia of pinion [kgm^2]	0.0004
Inertia of gear [kgm^2]	0.005
Radius of pinion [m]	30×10^{-3}
Radius of gear [m]	60×10^{-3}
Pinion teeth number	20
Gear teeth number	40
Gear ratio	2
Pinion base torque [Nm]	2
Gear torque [Nm]	4
Backlash [m]	40×10^{-6}
Torque amplitude [Nm]	0.8
NES inertia [kgm^2]	0.0004
NES damping c_N [Nms/rad]	0.002
Mesh damping ratio [-]	0.04

The NES was attached to the output shaft of the driven gear (Figure 7a) using an attachment shaft with a grub-screwed blind keyway. The NES rocker was fixed to this attachment, whereas the NES disk was supported by a ball bearing, allowing rotations of the disk with respect to its shaft. The rocker and the disk were connected via two thin steel shims, as shown in Figure 7b, realising the nonlinear restoring torque as it was described in Section 3. The speed of the gear and the NES were recorded using two Polytec© rotational laser vibrometers. Dedicated reflective tapes were adhered to the gear shaft and the NES, using, for the latter, a ring attached around the NES disk (Figure 7a,b). Data of the dynamic tests in the gear pair were collected at a sampling frequency of f_s = 8 kHz and analysed in MATLAB©.

3.2. Static Identification

The static torque of the NES was measured to verify the restoring torque predicted in Section 3 with the proposed design. The static identification test was conducted before the NES was installed on the gear pair assembly for dynamic testing, using the custom apparatus shown in the sketch in Figure 8. The NES attachment shaft was rigidly held in a vise. A lever was eccentrically attached on the back side of the NES disk in order to create a mechanical advantage for point B. Incremental weights were hanged from

point B, calculating the angular deflection of the NES disk at each increment based on measurements of h (Figure 8) and known trigonometric relations.

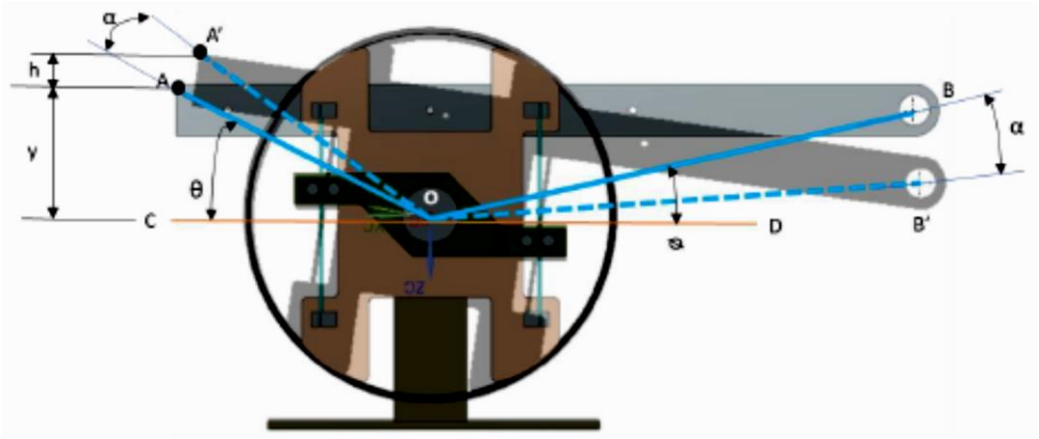

Figure 8. Sketch of the apparatus used to measure the static torque profile of the NES.

The static identification tests were repeated three times in each direction, clockwise and anti-clockwise, leading to the static restoring torque shown in Figure 9. The experimentally measured static torque of the NES was found to be in very good agreement with the torque profile predicted in Section 3. Note that Figure 9 compares the experimentally recorded static torque with the Taylor expansion in Equation (6). However, as was shown in Figure 6, Taylor expansions up to the fifth order both yield reasonably accurate expressions. This reaffirms confidence in the presented numerical approach in Section 2.

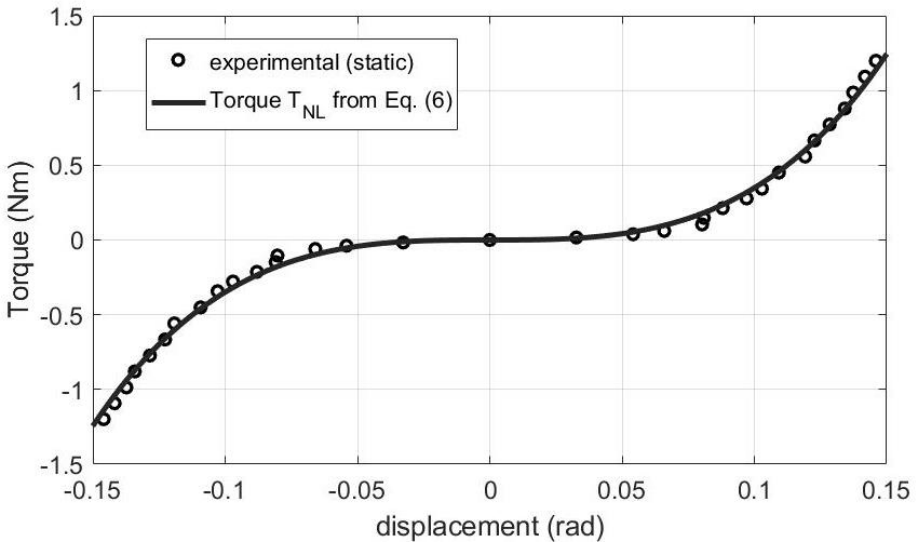

Figure 9. Theoretical torque curve computed with Equation (6) compared with statically identified torque profile given by Equation (6).

3.3. Gear Pair Dynamic Tests

Following the static identification of the NES restoring torque, the device was attached to the gear pair output shaft as described in the beginning of this section. The NES–gear assembly was then tested at different input pinion speeds between 700 rpm and 1000 rpm. The first order of the pinion shaft speed was used to excite gear vibrations across all tests.

First, the data were analysed to verify the restoring torque dynamically. The recorded NES speed was differentiated to compute the NES angular acceleration, and, knowing the NES inertia, the non-conservative restoring torque was computed. Figure 10 shows the

torque of the NES for four pinion speeds against the fluctuating part of the instantaneous angular position. The theoretical torque following the Taylor expansion up to the fifth order, shown in Equation (6), is also plotted to compare the experimental results.

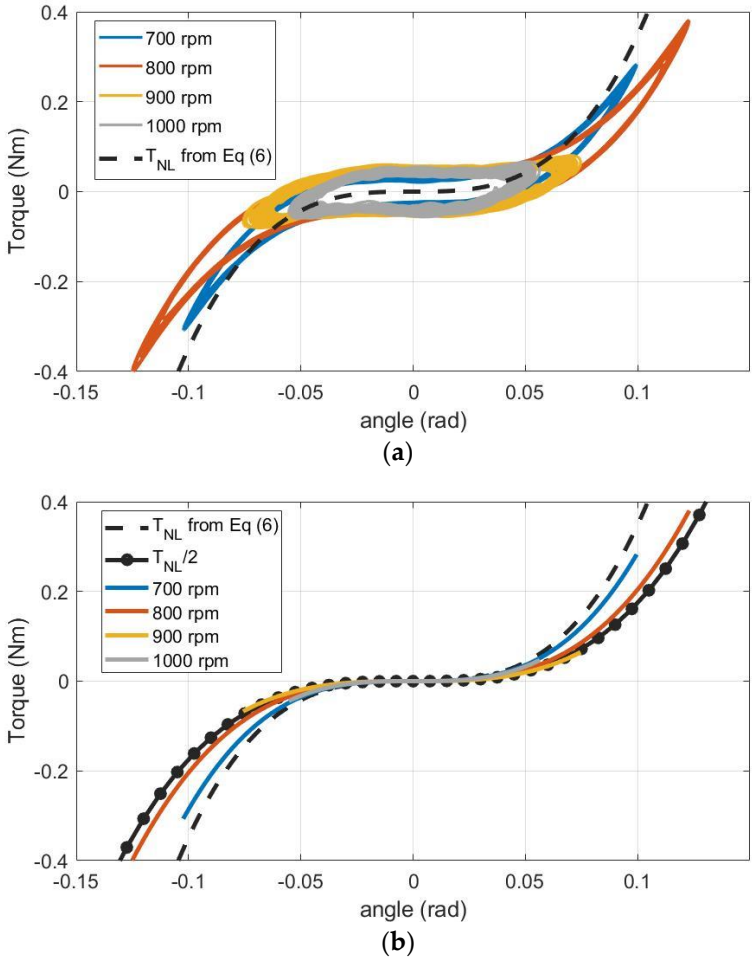

Figure 10. (**a**) Identification of the NES restoring torque computed from the experimental results for pinion speeds of 700, 800, 900 and 1000 rpm and comparison against the model results T_{NL} given by Equation (6); (**b**) elimination of damping from the restoring torque and comparison with NES model torque with two working shims (T_{NL}) and only one working shim ($T_{NL}/2$).

A significant deviation of these results from the predicted (and statically identified) torque is observed. This mismatch persists across the examined speed range, where the NES was activated and consequently forced to oscillate with relatively higher torques (700 rpm and 800 rpm), and in the range beyond its expected activation, where the NES oscillates with low angular amplitudes (900 rpm and 1000 rpm). Additionally, a weak linear component is also observed, particularly in the deactivated state. Upon examination of the device following the tests, the clamps holding the beam shims were found to rigidly keep the beams ends in place. The tests were repeated, and similar behaviour was observed. In order to investigate this unexpected response, damping was eliminated from the experimentally calculated restoring torque, leading to the stiffness torques plotted in Figure 10b. Note that the viscous linear damping was retained in the identification procedure to maintain its accuracy, but it was then analytically removed. The stiffness curves are plotted together with the nonlinear torque model T_{NL} given by Equation (6) and a hypothetical scenario in which only one of the shims is in contact with its rollers, thus reducing the effective stiffness of the NES to half ($T_{NL}/2$). This reveals that the NES stiffness agrees remarkably well with the one-shim scenario when it attains high oscillation amplitudes, as Figure 10b shows for the case of 800 rpm. This observation possibly indicates that imperfections in the

design realisation are aggravated by the intensive NES vibrations, leading to undesired malfunction of one of the shims.

4. Discussion

Based on these deductions, the numerical model is revisited to explore further agreement with the proposition than one of the shims has been malfunctioning during the experimental tests. Recalculation of the NES–gear system response in the examined frequency range with Equations (1)–(3) updated with the quintic stiffness torque given in Equation (6) leads to the amplitudes shown in Figure 11. The reduction in the nonlinear stiffness coefficient causes a significant shift in the jump-down frequency of the NES under the same damping conditions with the corresponding variation in the gear amplitudes. In fact, the numerical results are in good agreement with the experimentally recorded amplitudes, confirming that the NES was working with nearly half its effective stiffness. Combining this with the static identification leads to the conclusion that one of the NES shims was losing contact with the NES rocker. Nevertheless, and although the NES prototype did not follow the optimised response, the model results in Figure 11 prove the theoretical predictability of the NES design and, by extension, the expected optimised operation, should further refining modification be allowed.

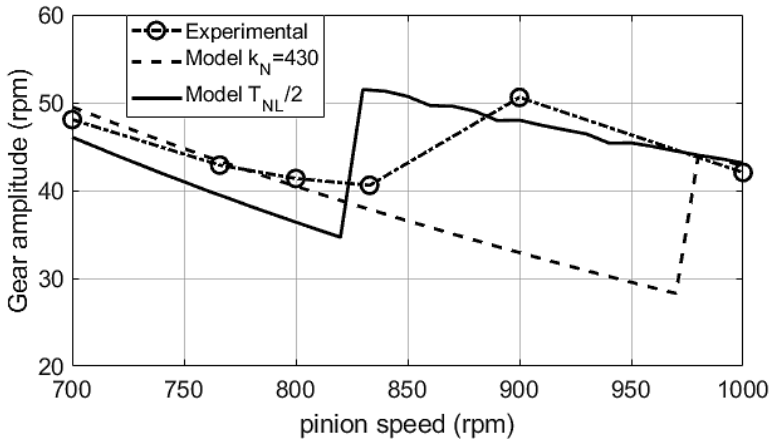

Figure 11. Experimental results of peak-to-peak gear amplitude compared with modelling results.

Further, Figure 12 compares the gear time history when the NES is active, with the gear response recorded with the NES in locked state for pinion speeds of 700 rpm, 800 rpm and 900 rpm. In Figure 12a,b, the active gear amplitude is found reduced, whereas in Figure 12c, it is found nearly unaffected by the presence of the NES. This expected behaviour is consistent with the modelling results and it is attributed to the NES action, as Figure 13 shows. The NES oscillation amplitude when the pinion runs at 800 rpm is significantly higher, leading to a reduction in the gear speed fluctuations. On the other hand, moving to 900 rpm, where the gear is shown to be almost unaffected, the NES is found to oscillate at very low amplitudes.

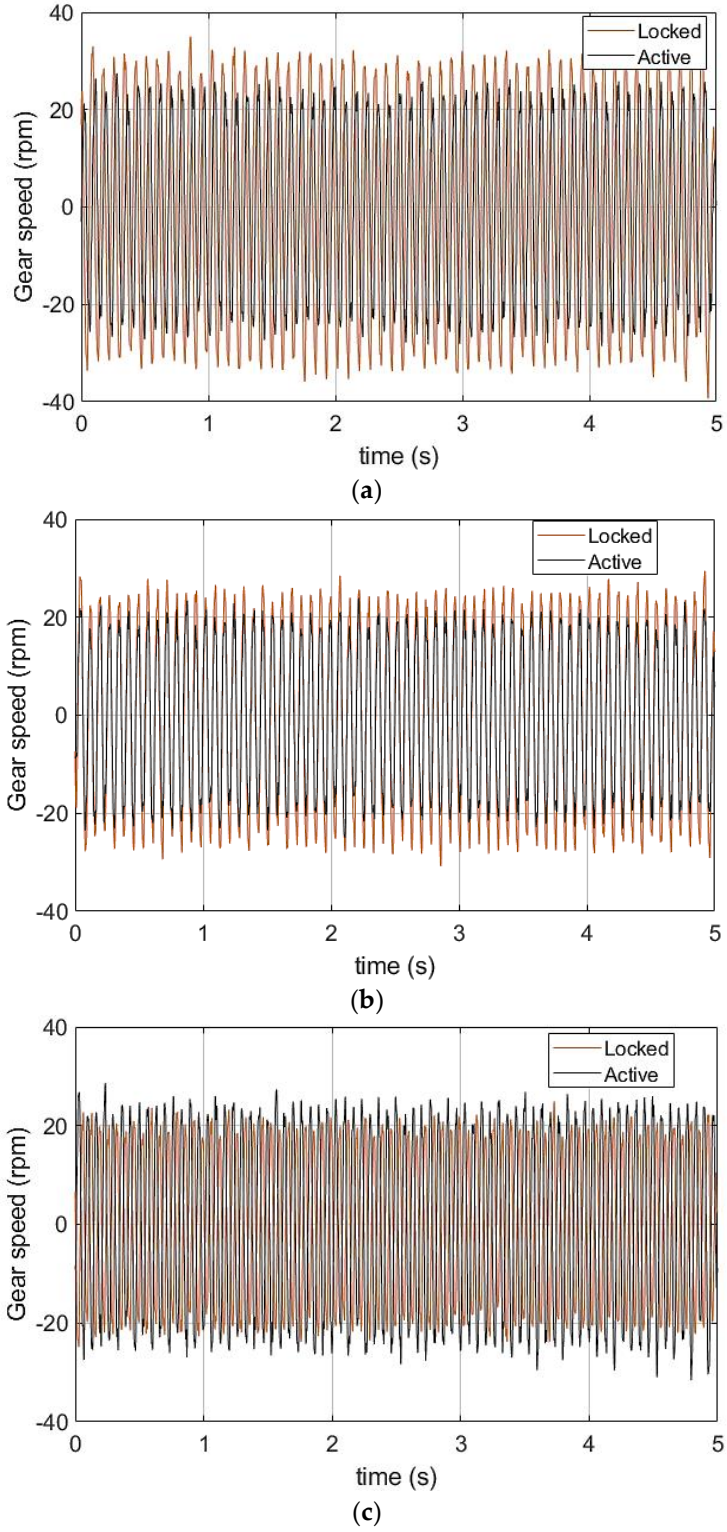

Figure 12. Time histories of the gear vibrations for active and locked NES and mean speed of the pinion; (**a**) 700 rpm; (**b**) 800 rpm; (**c**) 900 rpm.

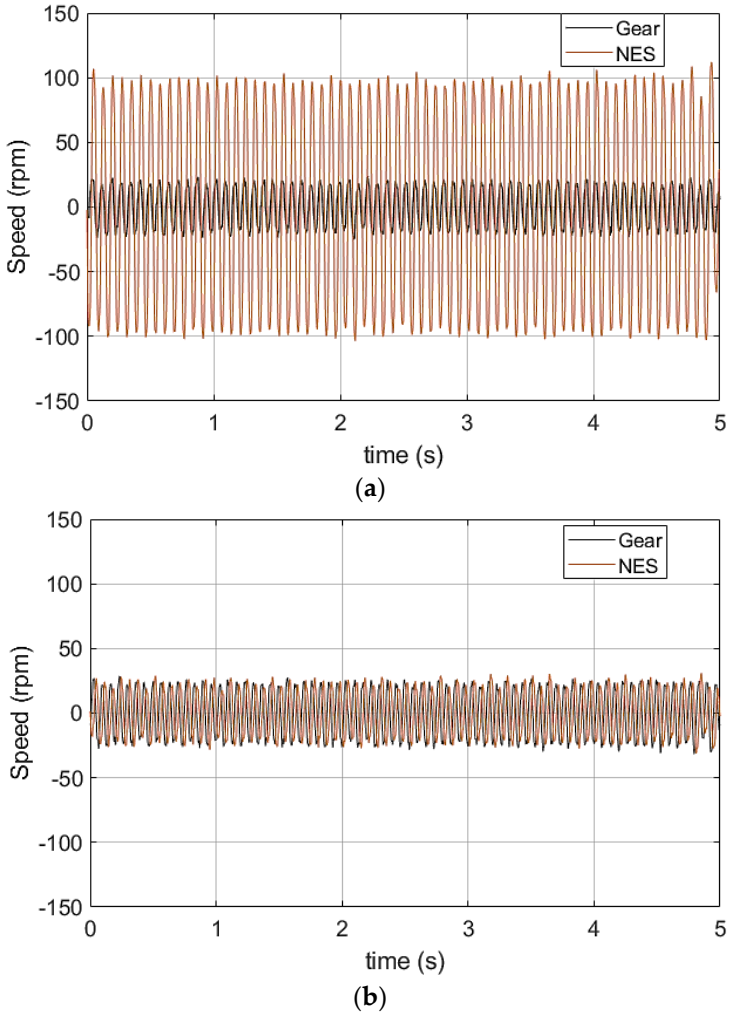

Figure 13. Time histories of the gear and the NES vibrations for active NES and mean speed of the pinion; (**a**) 800 rpm and (**b**) 900 rpm.

Last, the system energy is considered to further enhance the validation of the NES action. In Figure 14a, the NNM of the system lying within the frequency range of interest is plotted according to the initial design target as informed by the model in Section 2; the statically identified restoring torque was seen to closely match the design target, and the dynamically identified restoring torque was inferred to correspond to the partial malfunction of the prototype, with only one shim applying effective torque to the gear shaft. Juxtaposing the vibration energy of the system at different applied speeds shows that the system response is dictated by the influence of the NNM corresponding to $T_{NL}/2$. Additionally, calculation of the energy damped by the NES close to the observed activation range shows the significant transfer of energy to the NES, such as in the cumulative energy dissipated by the NES when the pinion speed was 700 rpm and 800 rpm, as shown in Figure 14b. The response of the system at these speeds corresponds to the reduced gear amplitudes that were observed in the frequency plot in Figure 11 and the time histories in Figure 12, with an expected drop in the dissipated energy when the NES moves out of its activation range to 900 rpm and 1000 rpm.

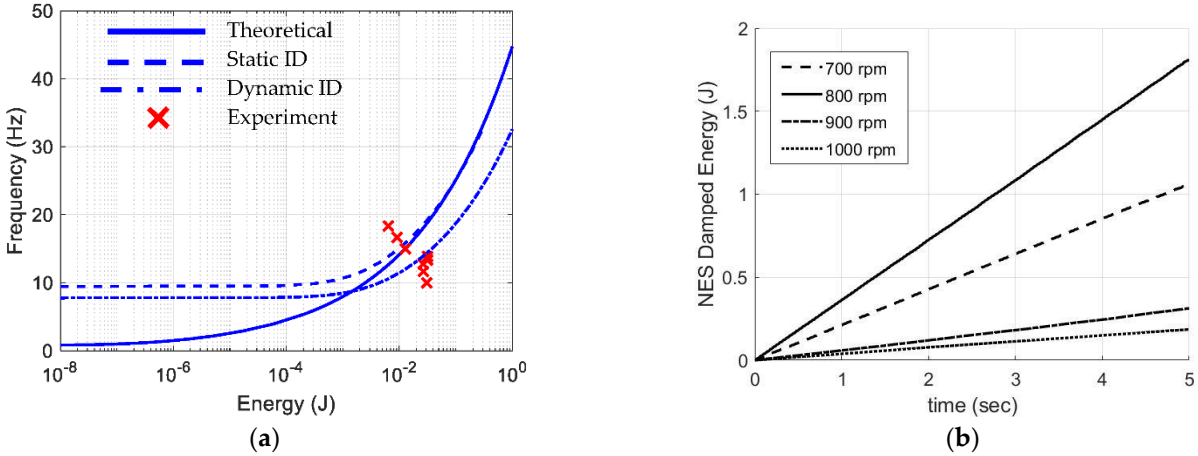

(**a**) (**b**)

Figure 14. (**a**) Comparison of theoretical NNMs (solid line) with NNM refined from static ID (dashed line), NNM refined from dynamic ID (dash-dot) and active system energies (red x); (**b**) cumulative energy damped by the NES.

Considering the results from Figures 11–14, the NES is shown to reduce the gear speed fluctuations in a manner predictable from and agreeing with the model. Despite the non-optimised operation of the physical prototype, the fundamental justification supporting the motivation of this experimental study is confirmed.

5. Conclusions

A rotational NES to absorb vibration energy from lightly loaded gear pairs has been designed (based on a previously discussed concept) and experimentally tested. Beams have been used to produce the desired essential nonlinearity within a realistic design space. Static and dynamic identification was conducted. The latter revealed that the NES stiffness closely agrees with the one-beam scenario at high oscillation amplitudes, which hints that design imperfections prevent the full realisation of the NES' expected performance. The resulting reduction in the nonlinear stiffness coefficient introduces a significant shift in the jump-down frequency of the NES with respect to the gear vibration amplitude variation. The NES was experimentally found to reduce the fluctuations of the gear pair output speed amplitude in a way that agrees with the predicted model results, verifying that the NES was operating with only half its effective nonlinear stiffness. Although the NES design has not been further optimised, the fundamental operation of the experiment confirms the motivation of this work.

Author Contributions: Investigation, B.F., P.A., S.L., S.T. and D.M.M.; Methodology, B.F., P.A., S.L. and S.T.; Supervision, S.T.; Validation, P.A. and S.L.; Writing—original draft, P.A. and S.T.; Writing—review and editing, B.F., P.A., S.T. and D.M.M. All authors have read and agreed to the published version of the manuscript.

Funding: This research was funded by EPSRC, grant number EP/L019426/1 (Targeted energy transfer in powertrains to reduce vibration-induced energy losses).

Data Availability Statement: The data presented in this study are available on request from the corresponding author. The data are not publicly available due to restrictions related to a potential patent application.

Conflicts of Interest: The authors declare no conflict of interest.

References

1. Turner, J.; Popplewell, A.; Patel, R.; Johnson, T. Ultra Boost for Economy: Extending the Limits of Extreme Engine Downsizing. *SAE Int. J. Eng.* **2014**, *7*, 387–417. [CrossRef]
2. De la Cruz, M.; Theodossiades, S.; Rahnejat, H. An Investigation of Manual Transmission Drive Rattle. *Proc. Inst. Mech. Eng. Part K J. Multi Body Dyn.* **2009**, *224*, 167–181. [CrossRef]

3. Theodossiades, S.; Tangasawi, O.; Rahnejat, H. Gear Teeth Impacts in Hydrodynamic Conjunctions Promoting Idle Gear Rattle. *J. Sound Vib.* **2009**, *303*, 632–658. [CrossRef]
4. Theodossiades, S.; Gnanakumar, M.; Rahnejat, H.; Kelly, P. Effect of a Dual–Mass Flywheel on the impact–induced noise in vehicular powertrain systems. *Proc. Inst. Mech. Eng. Part D J. Automobile Eng.* **2006**, *220*, 747–761. [CrossRef]
5. Alsuwaiyan, A.S.; Shaw, S.W. Performance and Dynamic Stability of General-Path Centrifugal Pendulum Vibration Absorbers. *J. Sound Vib.* **2002**, *252*, 791–815. [CrossRef]
6. Haris, A.; Motato, E.; Theodossiades, S.; Rahnejat, H.; Kelly, P.; Vakakis, A.; Bergman, L.; McFarland, D. A study on torsional vibration attenuation in automotive drivetrains using absorbers with smooth and non-smooth nonlinearities. *Appl. Math. Model.* **2017**, *46*, 674–690. [CrossRef]
7. Haris, A.; Motato, E.; Mohammadpour, M.; Theodossiades, S.; Rahnejat, H.; O' Mahony, M.; Vakakis, A.; Bergman, L.; McFarland, D. On the effect of multiple parallel nonlinear absorbers in palliation of torsional response of automotive drivetrain. *Int. Int. J. Non-Linear Mech.* **2017**, *96*, 22–35. [CrossRef]
8. Motato, E.; Haris, A.; Mohammadpour, M.; Theodossiades, S.; Rahnejat, H.; Kelly, P.; Vakakis, A.; Bergman, L.; McFarland, D.M. Targeted Energy Transfer and Modal Energy Redistribution in Automotive Drivetrains. *Nonl. Dyn.* **2017**, *87*, 169–190. [CrossRef]
9. Haris, A.; Alevras, P.; Mohammadpour, M.; Theodossiades, S.; O' Mahony, M. Design and validation of a nonlinear vibration absorber to attenuate torsional oscillations of propulsion systems. *Nonl. Dyn.* **2020**, *100*, 33–49. [CrossRef]
10. Dolatabadi, N.; Theodossiades, S.; Rothberg, S.J. Design Optimization Study of a Nonlinear Energy Absorber for Internal Combustion Engine Pistons. *ASME J. Comp. Nonl. Dyn.* **2018**, *13*, 090910-1–090910-12. [CrossRef]
11. Dolatabadi, N.; Theodossiades, S.; Rothberg, S.J. Passive Control of Piston Secondary Motion using Nonlinear Energy Absorbers. *ASME J. Vib. Acoust.* **2017**, *139*, 051009-1–051009-12. [CrossRef]
12. Vakakis, A.; Gendelman, O.V.; Bergman, L.A.; McFarland, D.M.; Kerschen, G.; Lee, Y.S. *Nonlinear Targeted Energy Transfer in Mechanical and Structural Systems: Solid Mechanics and Its Applications*, 1st ed.; Springer: Dordrecht, The Netherlands, 2008.
13. Gendelman, O.; Manevitch, L.I.; Vakakis, A.F.; M'Closkey, R. Energy Pumping in Nonlinear Mechanical Oscillators: Part I—Dynamics of the Underlying Hamiltonian Systems. *J. Appl. Mech.* **2001**, *68*, 34–41. [CrossRef]
14. Vakakis, A.F.; Gendelman, O. Energy Pumping in Nonlinear Mechanical Oscillators: Part II—Resonance Capture. *J. Appl. Mech.* **2001**, *68*, 42–48. [CrossRef]
15. Kerschen, G.; Vakakis, A.F.; Lee, Y.S.; McFarland, D.M.; Kowtko, J.J.; Bergman, L.A. Energy Transfers in a System of Two Coupled Oscillators with Essential Nonlinearity: 1:1 Resonance Manifold and Transient Bridging Orbits. *Nonl. Dyn.* **2005**, *42*, 283–303. [CrossRef]
16. McFarland, D.M.; Kerschen, G.; Kowtko, J.J.; Lee, Y.S.; Bergman, L.A.; Vakakis, A.F. Experimental Investigation of Targeted Energy Transfer in Strongly and Nonlinearly Coupled Oscillators. *J. Acoust. Soc. Amer.* **2005**, *118*, 791–799. [CrossRef]
17. Kerschen, G.; Lee, Y.S.; Vakakis, A.F.; McFarland, D.M.; Bergman, L.A. Irreversible Passive Energy Transfer in Coupled Oscillators with Essential Nonlinearity. *SIAM J. Appl. Math.* **2005**, *66*, 648–679. [CrossRef]
18. Vakakis, A.F.; Manevitch, L.I.; Gendelman, O.; Bergman, L.A. Dynamics of linear discrete systems connected to local, essentially non-linear attachments. *J. Sound Vib.* **2003**, *264*, 559–577. [CrossRef]
19. Lund, A.; Dyke, S.J.; Song, W.; Bilionis, I. Identification of an experimental nonlinear energy sink device using the unscented Kalman filter. *Mech. Syst. Sign. Proc.* **2020**, *136*, 106512. [CrossRef]
20. Javidialesaadi, A.; Wierschem, N.E. An inerter-enhanced nonlinear energy sink. *Mech. Syst. Sign. Proc.* **2019**, *129*, 449–454. [CrossRef]
21. Zhang, Y.W.; Lu, Y.N.; Zhang, W.; Teng, Y.Y.; Yang, H.X.; Yang, T.Z.; Chen, L.Q. Nonlinear energy sink with inerter. *Mech. Syst. Sign. Proc.* **2019**, *125*, 52–64. [CrossRef]
22. Yao, H.; Wang, Y.; Xie, L.; Wen, B. Bi-stable buckled beam nonlinear energy sink applied to rotor system. *Mech. Syst. Sign. Proc.* **2020**, *138*, 106546. [CrossRef]
23. Viguié, R.; Kerschen, G.; Golinval, J.C.; McFarland, D.M.; Bergman, L.A.; Vakakis, A.F.; van de Wouw, N. Using passive nonlinear targeted energy transfer to stabilize drill-string systems. *Mech. Syst. Sign. Proc.* **2009**, *23*, 148–169. [CrossRef]
24. Gendelman, O.V.; Sigalov, G.; Manevitch, L.I.; Mane, M.; Vakakis, A.F.; Bergman, L.A. Dynamics of an Eccentric Rotational Nonlinear Energy Sink. *J. Appl. Mech.* **2012**, *79*, 011012-1–011012-9. [CrossRef]
25. Hubbard, S.A.; McFarland, D.M.; Bergman, L.A.; Vakakis, A.F.; Andersen, G. Targeted Energy Transfer between a Swept Wing and Winglet-Housed Nonlinear Energy Sink. *AIAA J.* **2014**, *52*, 2633–2651. [CrossRef]
26. Scagliarini, G.; Viguié, R.; Kerschen, G.; Pellicano, F. Spur Gear Vibration Mitigation by Means of Energy Pumping. In Proceedings of the IMAC-XXVII, Orlando, FL, USA, 9 February 2009.
27. Friskney, B.; Motato, E.; Haris, A.; Mohammadpour, M.; Theodossiades, S. A Study on Attenuating Gear Teeth Oscillations at Low Engine Speeds Using Nonlinear Vibration Absorbers. *SAE Tech. Pap.* **2018**. [CrossRef]